THE JOURNAL OF PHYSICAL CHEMISTRY C

Article

pubs.acs.org/JPCC

Time−Energy Uncertainty and Electronic Correlation in H^+−Graphite Collisions

Fernando J. Bonetto,*[,†,‡] Marcelo A. Romero,[†] Adalberto Iglesias-García,[†] Ricardo A. Vidal,[†,§] and Edith C. Goldberg[†,‡]

[†]Instituto de Física del Litoral (CONICET - UNL), Güemes 3450, S3000GLN Santa Fe, Argentina

[‡]Departamento Ing. Materiales, Facultad de Ing. Química (UNL), Santiago del Estero 2829, S3000AOM Santa Fe, Argentina

[§]Departamento de Física, Facultad de Ing. Química (UNL), Santiago del Estero 2829, S3000AOM Santa Fe, Argentina

Supporting Information

ABSTRACT: The formation of negative ions in the scattering of protons by a highly oriented pyrolytic graphite (HOPG) surface is theoretically and experimentally analyzed for a large scattering angle and compared with previous results obtained in the same system but for a forward scattering geometry. These experiments were motivated by the fact that the interaction of a hydrogen atom with a surface is the prototype system for studying the intra-atomic Coulomb repulsion in an s-like valence orbital localized in the atom. We tried to answer the open questions related to the electronic correlation effects and the influence of the detailed surface band structure by using appropriate theoretical models. The comparison with the experiment of theoretical results obtained by using different limit approximations of the electronic repulsion in the atomic state shows the expected validity ranges according to the ion velocity. However, the most remarkable conclusion obtained from this comparison is the nonvalidity of an adiabatic picture of the energy levels shifted by the interactions with the surface atoms, when the energy uncertainty introduced by the ion velocity becomes of the order of the electronic repulsion in the hydrogen ground state.

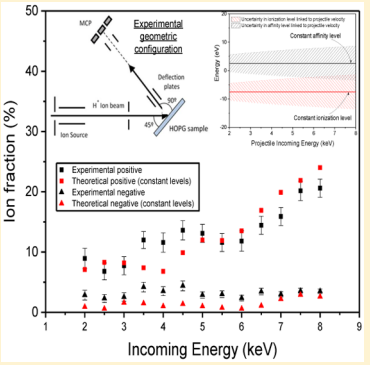

1. INTRODUCTION

Charge exchange between an atomic projectile and a target surface during a nonequilibrium collision process is a topic of relevance for extensive areas involving basic and applied research. The tunnelling of resonant electrons is crucial to understand and describe charge transfer between ions and various surfaces. An abundance of literature exists exploring these systems, but the mechanisms that control the charge exchange between them are not yet completely understood.[1−27]

The interaction of hydrogen ions with solid surfaces is not only relevant for fundamental science but also important in devices involved in plasma confinement.[28−30] On the other side, graphite is also important for fusion physics for being the first wall material in a Tokamac variable configuration. However, only a few groups have studied the ion formation after scattering from graphite.[22,25,27,28,31−35]

When working with charge exchange during a scattering process, i.e., electronic transfer to and from a target surface to a colliding ion, it is important to consider that the projectile electronic energy levels are shifted and broaden with respect to the energy level at large distances. This effect is primarily due to the interaction of the projectile states with the conduction band and with the target inner states.[36,37]

Previous studies of proton scattering by a highly oriented pyrolytic graphite (HOPG) surface[22,25,31,32,38−40] have shown that questions about the electronic correlation effects and the influence of the fine details of the surface band structure still remain open. The formation of hydrogen negative ions requires an electron capture from the surface band states to the affinity state, depending, therefore, on the characteristics of the surface band structure around the Fermi level and on the level shift due to the ion−surface interaction. In contrast, the neutralization process, involving the projectile ionization level situated below the surface Fermi energy and well immersed within the surface valence band, is not expected to be highly sensitive to these characteristics. Nevertheless, the correlation between the different charge states introduced by the electronic interaction within a time-dependent evolution of the colliding system may lead to no intuitive results.

In a previous work,[22] the negative and positive ion fractions in the scattering of protons by HOPG were measured within a forward scattering geometry, and the theoretical calculation of the ion fractions was based on an infinite correlation limit. In this work, it was suggested that the differences found between theoretical and experimental data were due to electronic correlation effects and to electronic structure details not taken into account by considering only the diagonal terms of the density matrix of the solid.

Received: November 12, 2014
Revised: January 7, 2015

DOI: 10.1021/jp511339v
J. Phys. Chem. C XXXX, XXX, XXX−XXX

In our previous works,[22,25,40] under forward scattering (FS) conditions, we took into account many different surface atoms along the ion trajectory. Then, mainly due to computational time, it was impossible to consider a finite electronic repulsion U and to take into account fine band structure details. However, these ingredients can be incorporated in a theoretical description of a dynamic collision process when a backscattering (BS) geometry is analyzed. Under this condition, we expect only a reduced and controlled number of surface atoms which effectively interact with the ion projectile.[24]

In the present work, theoretical calculations based on an Anderson model[41] and a time-dependent Green function formalism[42] are used for describing the novel measurements of the positive and negative ion fractions when H^+ projectiles are backscattered by a highly oriented pyrolytic graphite surface (HOPG). Our theoretical description includes now sophisticated elements such as a finite electronic repulsion in the localized state and the complete density matrix of the solid. The theoretical–experimental data assessment allows us to infer how relevant are the different physical ingredients contemplated in the model and the energy range where they play a significant role.

2. ION FRACTION MEASUREMENT: EXPERIMENTAL SETUP

Charge transfer experiments were performed in the low-energy ion-scattering time-of-flight (LEIS-TOF) system available in our group. Basically, it consists of an ultrahigh vacuum (UHV) chamber with a base pressure in the 10^{-9} Torr range; an ion gun that includes a Colutron ion source, focusing lens, a Wien filter, and pulsing plates; and a time-of-flight (TOF) spectrometer.

The positive hydrogen ions are produced in a discharge source (Colutron). Subsequently, they are accelerated to the chosen energy, and a Wien filter is used to separate H^+ from other sorts of ions. A pulsed ion beam is produced afterward by applying a square-wave voltage to a pair of deflection plates located in front of a rectangular slit. The pulsed ion beam is then scattered by the HOPG substrate.

The HOPG sample was cleaned in UHV by annealing at 1300 K for 5 min. The sample is kept at around 500 K during the whole experiment to prevent it from potential contamination with implanted ions. The cleaning process was repeated after each experiment.

The energy distributions of the ions and neutrals (H^+, H^-, and H^0) scattered off the graphite surface were obtained by time-of-flight methods.[37,43] The detector essentially consists of three electrodes (anodes) placed behind two microchannel plates (MCPs) mounted in a chevron configuration at the end of the drift tube. To measure neutrals, scattered ions are filtered off by a pair of deflection plates placed at the drift tube entrance (see Figure 1), and the central electrode is used to detect the neutral particles. To measure the scattered ions (H^+ or H^-) a previously calibrated voltage is applied to a second set of deflection plates mounted in front of the microchannel plates, and one of the outer anodes is used to detect them. By selecting the elastic peak from both neutrals and H^+ (or H^-) spectra, the positive and negative ion fractions can be straightforwardly calculated. The incoming energy was varied from 2 to 8 keV, with a 500 eV step.

The sample–detector distance is 137 cm, and the ingoing/exit angles were fixed to 45°/90°, measured with respect to the HOPG surface plane (total scattering angle: 135°). This geometry was particularly chosen to ensure consistency with the theoretical model assumptions/constraints.

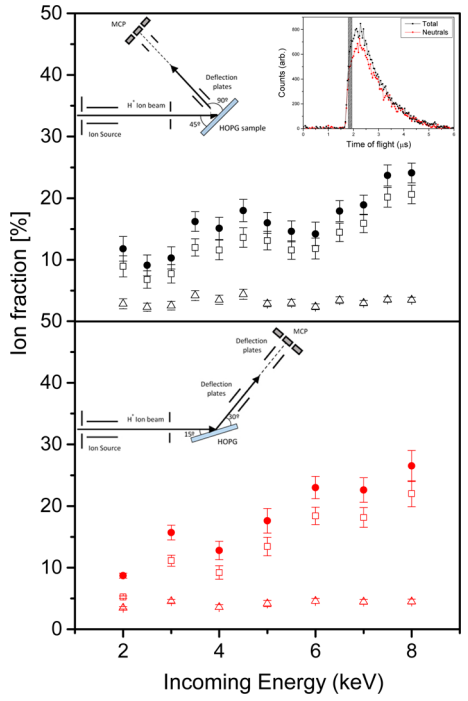

Figure 1. Present measurements (backscattering conditions, upper panel) are compared with the forward scattering measurements of ref 22. The corresponding experimental geometries are sketched (insets, left). The total (ions plus neutrals) and neutral scattered particle LEIS-TOF spectra corresponding to BS geometry and 8 keV incoming energy are shown (right inset, upper panel), and the elastic peak region considered is specified (shadowed gray region). Empty squares and triangles represent positive and negative ion fractions, respectively. Full circles denote the total ion fractions measured, the sum of positive and negative ion fractions.

3. RESULTS AND THEORY

In Figure 1 the positive and negative ion fractions of the backscattered projectiles are contrasted with our previous measurements[22] on the same system obtained in a forward scattering configuration (scattering angle: 45°, incoming angle: 15°). The ion fractions are plotted as a function of the incoming energy, and the geometry used is sketched.

In Figure 1 we can observe that similar ion fractions were obtained for both scattering configurations. Negative ion fractions are lower than 5% and slightly dependent on the incoming energy. Positive ion fractions increase with incoming energy and vary between 5 and 20%. The remarkable matching found between both experimental data is unexpected given the substantial physical differences between both collision configurations. For instance, in FS the perpendicular component of the incoming energy, E^{in}_{perp}, varies from 134 to 536 eV, while in BS it ranges from 1000 to 4000 eV. Thus, the time during which the proton is in contact with the surface, along the incoming trajectory, is much longer when the FS configuration is used. The perpendicular exit energies differ by a factor of 3; E^{exit}_{perp} varies between 475 and 1900 eV in FS, while in BS it ranges from 1500 to 6000 eV.

Appropriate theoretical proposals able to describe the experimental trends observed could reveal the underlying physics of charge exchange during H^+–HOPG collisions.

DOI: 10.1021/jp511339v
J. Phys. Chem. C XXXX, XXX, XXX–XXX

We will briefly review the main points of the theoretical aspects in the following paragraphs.

The interaction of a hydrogen atom with a surface is the prototype system for studying the intra-atomic Coulomb repulsion in an s-like valence orbital localized in the atom. The Anderson Hamiltonian provides an adequate description of the negative and positive ion fractions in the time-dependent collision process

$$H = \sum_{\vec{k},\sigma} \varepsilon_{\vec{k}} \hat{n}_{\vec{k},\sigma} + \sum_{\sigma} \left[\varepsilon_I + \frac{U}{2} \hat{n}_{a-\sigma} \right] \hat{n}_{a\sigma} + \sum_{\vec{k},\sigma} [V_{a,\vec{k}} \hat{c}^{+}_{a,\sigma} \hat{c}_{\vec{k},\sigma} + \text{h.c.}] \quad (3.1)$$

The first term in eq 3.1 corresponds to the diagonalized solid with eigenstates $\varepsilon_{\vec{k}}$ and occupation number operators $\hat{n}_{\vec{k},\sigma}$, σ being the electron spin projection. The second term of 3.1 describes the atom s-valence state with ionization energy ε_I and a Coulomb repulsion U; $\hat{n}_{a\sigma}$ is the atom state occupation number operator. The interaction between the solid ($\vec{k}$) and atom (a) states is described by the third term of eq 3.1.

In a purely stationary problem, the most appropriate approximated solution of eq 3.1 depends on the relation between the correlation parameter U and the level width originated in the atom−surface interaction

$$\Gamma(\varepsilon_I) = \pi \sum_{\vec{k}} |V_{a,\vec{k}}|^2 \delta(\varepsilon_I - \varepsilon_{\vec{k}})$$

The approximations based on a large value of U are valid if $\Gamma(\varepsilon_I) \ll U$ (weak coupling limit). The opposite limit, small values of U, is suitable when $\Gamma(\varepsilon_I) \gg U$ (strong coupling limit).

In time-dependent scattering processes, assuming a level width Γ that decays with the atom−surface distance, and a practically constant correlation parameter U, both strong and weak coupling situations can be thought to occur in different regions of the ion trajectory.

However, in a dynamical scattering process the time−energy uncertainty relation $\Delta E_{un} \approx \hbar/2\tau$ (where τ is the characteristic time of evolution of an unstable state) should also be considered. Thus, as it is well-known, the energy of an unstable state cannot be determined with arbitrary accuracy but only to within an energy uncertainty ΔE_{un}, called the natural width of the state.[44] In an ion−surface collision process, $\Delta E_{un} \approx \nu_\perp/2$ in atomic units, where $\nu_\perp$ is the perpendicular component of the ion velocity.[45] Therefore, the time-dependent process introduces an effective decrease in the energy difference between the ionization and the affinity levels (U) as ΔE_{un} increases. Then, we can define an effective correlation parameter $U^* = U - 2\Delta E_{un}$. In Figure 2 we show the one electron levels, their variations due to the adiabatic interaction with the surface, and the width ΔE_{un} (represented by the "error bars" of height equal to $2\Delta E_{un}$) introduced by the time−energy uncertainty relation.

The different regimes are then determined by the relation between the effective correlation parameter U^* and the level width introduced by the interaction Γ, which is calculated as an effective value in the range of projectile−surface distances at which the charge exchange occurs. In this way, we have three different limit situations:

- $U^* \gg \Gamma$: either an infinite U limit or a spinless approximation have to work well if the incoming velocity is low enough to assume a neutral hydrogen as the initial condition for the dynamical evolution. In both approximations

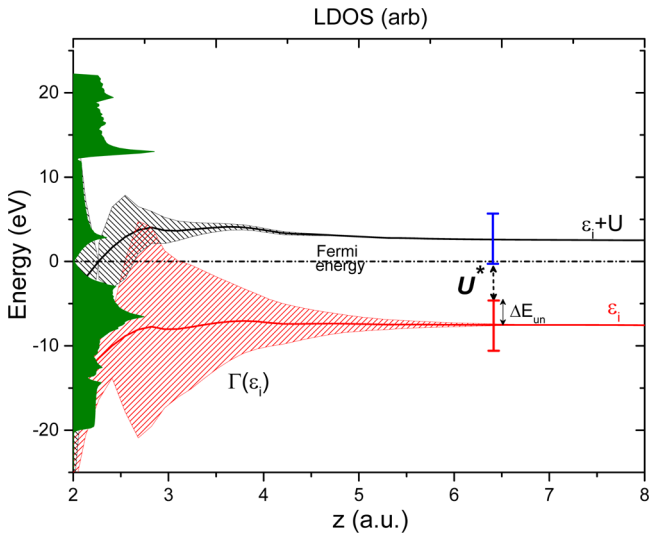

Figure 2. Ionization (red) and affinity (black) one-electron levels of the projectile are plotted with their respective widths Γ due to the interaction with the HOPG surface (red and black shadowed region). At distances closer to the surface (z < 8 au), the shifting of the energy levels is mainly caused by short-range interactions. These interactions are calculated within a mean field approximation[16] and considering the atom charges frozen at their values for the noninteracting system. The widths introduced by the uncertainty in the projectile velocity, corresponding to a 2 keV incoming energy in a BS experiment, are represented by red and blue error bars. The HOPG density of states (green) is also depicted.

the charge fluctuations $H^0 \leftrightarrow H^+$ and $H^0 \leftrightarrow H^-$ are treated separately,[22] by considering the ionization and the affinity levels as the active level in each case. To compare the theoretical calculations with experimental positive (Γ^+) and negative (Γ^-) ion fractions, we proposed[22]

$$\Gamma^+ = P^+(1 - P^-)$$
$$\Gamma^- = P^-(1 - P^+) \quad (3.2)$$

where P^+ and P^- are, respectively, the positive and negative ionization probabilities of initial neutral atoms.

- $U^* > \Gamma$: a large but finite U limit approximation is valid. In this case the calculation of the three possible charge states of hydrogen (H^+, H, H^-) is performed by using a second order in the coupling term $V_{a,\vec{k}}$ criteria to close the equation of motions that determine the appropriate Green functions.[46]
- $U^* < \Gamma$: a small-U limit approximation is the adequate one. The calculation of the three possible charge states of hydrogen (H^+, H, H^-) is performed by using perturbation theory up to a second order in the parameter U.[47,48] This approximation has been proven to be valid also for $U^* \approx \Gamma$.[47]

These different situations emerge in our experiments depending on the geometry of the experimental setup (FS or BS) as we will analyze in the following.

In our forward scattering experiment, the incoming perpendicular energies range from 134 to 536 eV, much smaller than the exit perpendicular energies that vary between 475 and 1900 eV. In this situation, we can assume that the proton has been neutralized along the incoming path, and therefore, the charge state of the projectile is completely defined along the outgoing part of the trajectory. In the region of relatively large distances to the surface (z > 5 au), the separation between the one-electron levels (ionization and

DOI: 10.1021/jp511339v
J. Phys. Chem. C XXXX, XXX, XXX−XXX

affinity) is larger than 10 eV (see Figure 2), and the average uncertainty introduced by the velocity is between 1.5 and 3 eV, as we can see from Figure 3. Then, in this situation $U^* > \Gamma$, and

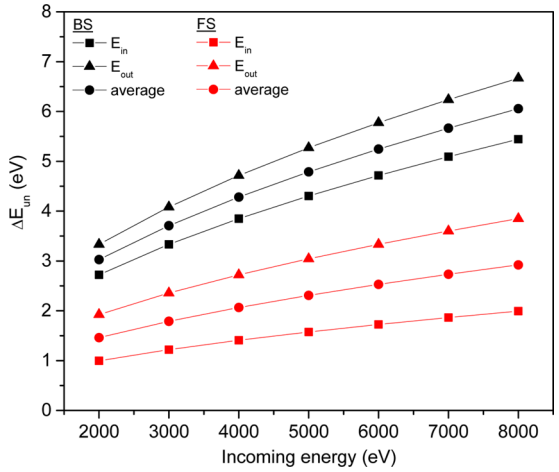

Figure 3. ΔE_{un} plotted as a function of the incoming energy. ΔE_{un} was calculated by considering the velocity corresponding to the perpendicular component of the incoming (ν_{perp}^{in}, full squares) and the exit velocity of the projectile (ν_{perp}^{exit}, full triangles). The average of them ($(\nu_{perp}^{in} + \nu_{perp}^{exit})/2$, full circles) is also shown. Black/red symbols correspond to BS/FS experimental setup.

therefore, it is reasonable that an approximation based on an infinite U limit or, moreover, one which ignores the electron spin leads to a rather satisfactory description of the ion fractions measured in the FS experimental geometry.[22] In this case we are referring to positive and negative ionization processes occurring near the surface, along the exit trajectory. Thus, they are more probable for larger exit projectile velocities.

It is also expected that this approximation does not provide a good description as the exit energy increases due to the decrease of U^* and to a less efficient neutralization along the incoming path.

In backscattering experiments, the situation radically changes. The perpendicular components of the ingoing and exit energies are larger than 1 keV, and then, the system is no longer in a very slow motion regime that allows for an effective neutralization along the incoming trajectory. Thus, a more relevant role played by the whole trajectory is envisioned. Under BS conditions, the relation $\Delta E_{un} \geq 3$ eV is fulfilled (see Figure 3). This leads to lower U^* values turning, in this way, the spinless approximation inadequate to reproduce BS experimental results. This conjecture is proven when spinless calculations are compared with BS experimental data as shown in Figure 4.

Effectively, the spinless approximation does not reproduce the BS experimental ion fraction trends and/or magnitudes. The good description of the positive ion fraction for incoming energies lower than 5 keV is only fortuitous, considering the approach used to determine the ion fractions under this approximation (eq 3.2).

In Figures 5(a) and 5(b) we show the ion fractions calculated under the large- (but finite) and the small-U limit approximations, respectively. It can be noticed that both approximations reproduce experimental data reasonably well for incoming energies below 5 keV. However, and especially for higher energies, a better description is achieved when using the

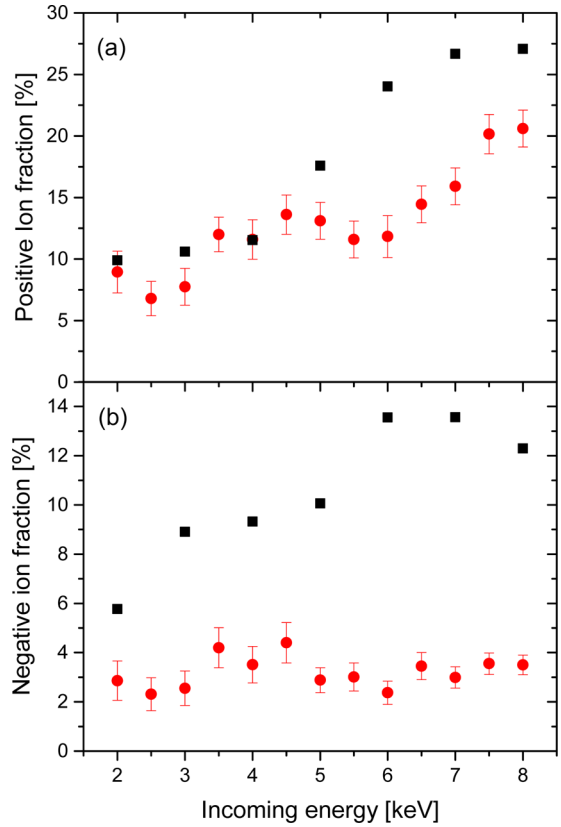

Figure 4. Backscattering experimental ion fractions (full circles) as a function of the incoming proton energy (incoming angle: 45°, exit angle: 90°), compared with spinless calculations (full squares).[22] (a) Positive ion fractions; (b) negative ion fractions.

small-U limit calculation. As discussed above, this is a consequence of a reduced U^* for this energy range.

It is clear that both ion fractions are overestimated for energy values larger than 4 keV, under the small-U assumption. Specifically, this difference is more pronounced for the negative ion fraction. A possible explanation for this finding might be given by Figure 6. Here, we depict the ionization and affinity energy level widths introduced by the projectile velocity (plotted as shadowed regions) as a function of the incoming energy. The constant values assumed for the ionization and affinity levels are calculated as an average of the adiabatic levels for projectile−surface distances in the 4−8 au region, where the interaction is still operative for charge exchange (see inset of Figure 6). In this figure we can see that both energy levels start to overlap at a projectile incoming energy around 5.5 keV. As stated above, this result could be strongly linked to the departure from experimental data exhibited at higher projectile incoming energies (Figure 5).

Figure 6 clearly indicates that for high projectile energies in the BS experimental configuration the level widths associated with the time−energy uncertainty cause overlapping of ionization and affinity levels in the whole range of projectile−surface distances. This special circumstance, primarily inherent to the projectile H, the geometric experimental configuration, and the incoming projectile energy, makes it impossible to clearly define the one-electron levels for the first and second electrons. In this special case, the concept of well-separated one-electron levels adiabatically varying due to the interaction with the surface appears intuitively erroneous.

DOI: 10.1021/jp511339v
J. Phys. Chem. C XXXX, XXX, XXX−XXX

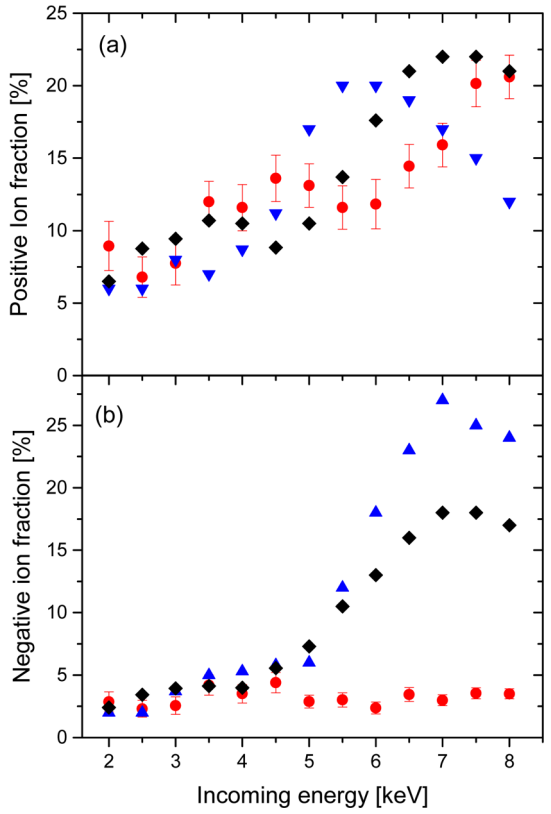

Figure 5. Theoretical calculations using the large-U limit (blue) and the small-U limit (black) are contrasted with experimental data (red).

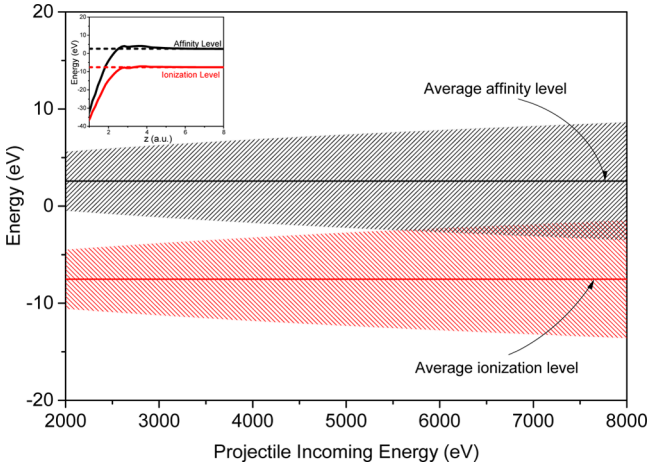

Figure 6. Ionization and affinity one-electron levels and their average width ΔE_{un} (represented by red and black shadowed regions of height equal to $2\Delta E_{un}$, respectively) are plotted as a function of the projectile incoming energy for the BS configuration. Inset: Ionization and affinity constant values are calculated as the average of the corresponding adiabatic levels (solid lines, inset) for projectile−surface distances in the 4−8 au region (dotted lines in the inset of this figure).

To test this idea, we decided to assume constant ionization and affinity levels along the ion trajectory. These constant levels were chosen to be equal to the corresponding values for the isolated hydrogen atom. The obtained results are shown in Figures 7(a) and 7(b). We obtain a fair description of the experimental results for the largest incoming energies. The remaining differences may still be due to the limited number of C atoms and the nonfully realistic proton trajectory we have

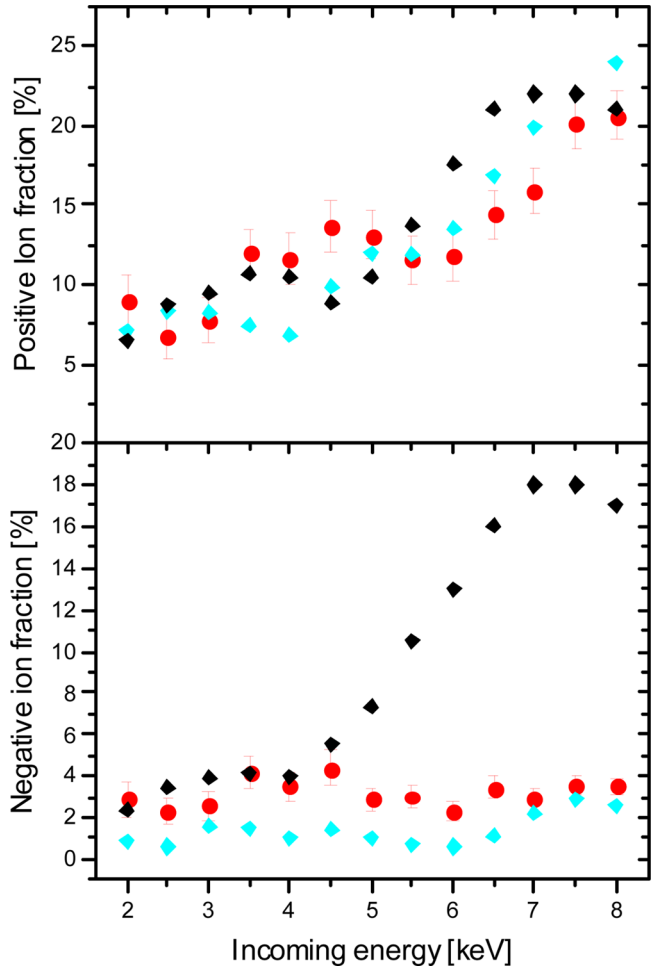

Figure 7. Theoretical calculations using the small-U limit (black) and the constant level approximation (cyan) are compared with experimental data (red).

considered in the calculations, as it is discussed in the following section.

Results shown in Figure 7 strongly suggest that the theoretical approach including the small-U limit approximation plus ionization and affinity constant levels assumption is adequate to accurately describe positive and negative ion fractions under these particular conditions.

4. DETAILS OF THE CALCULATION

The atom−surface coupling terms and the energy shift of the projectile energy levels due to short- and large-range interactions are calculated by following the same considerations as in refs 22 and 25. The model calculation is based on an expansion of the solid states $\phi_{\vec{k}}(\vec{r})$ in the atomic states $\varphi_\alpha(\vec{r} - \vec{R}_i)$ centered on the different atoms of the solid (α denotes the orbital type and $\vec{R}_i$ the position with respect to the scatter atom). In this way the coupling term $V_{\vec{k}a}(= V_{\vec{k}a})$ can be written as

$$V_{\vec{k}a}(\vec{R}) = \sum_{\alpha,i} c_{\alpha,i}^{\vec{k}} V_{\alpha i,a}^{\dim}(\vec{R} - \vec{R}_i) \tag{4.1}$$

where $V_{\alpha i,a}^{\dim}(\vec{r} - \vec{R}_i)$ is the atomic coupling between the α-states of the i-atom of the solid and the state of the projectile positioned at the distance $\vec{R}$ from the scatter atom, calculated by using a mean field approximation and a symmetrically

DOI: 10.1021/jp511339v
J. Phys. Chem. C XXXX, XXX, XXX−XXX

orthonormalized atomic basis set in the space of the dimmer projectile-solid atom.[49] The coefficients $c^{\vec{k}}_{\alpha,i}$ in the expansion 4.1 define the density matrix of the solid given by the expression

$$\rho_{i,j,\alpha,\beta}(\varepsilon) = \sum_{\vec{k}} c^{\vec{k}}_{\alpha,i} c^{\vec{k}}_{\beta,j} \delta(\varepsilon - \varepsilon_{\vec{k}}) \tag{4.2}$$

The calculations by assuming either a large but finite U or a small U were performed by considering a perpendicular trajectory of the proton with a velocity equal to the normal component, according to the scattering geometry of the experiment (scattering angle of 135° and an incoming angle of 45° with respect to the surface). The energy loss in the binary collision is also taken into account ($E_{out} = 0.75E_{in}$). Only the scatter atom ($\vec{R}_0 = (0,0,0)$) and its first three neighbors on the surface were considered in the expansion 4.1 because of the complexity of the computational task. Then, the results shown in Figures 5 and 7 correspond to the respective U limit calculation including these four C atoms and the complete density matrix in this subspace of neighbors.

We test the previous assumptions by performing a comparative analysis of the ionization probabilities in the spinless calculation. In Figure 8 we show that a perpendicular

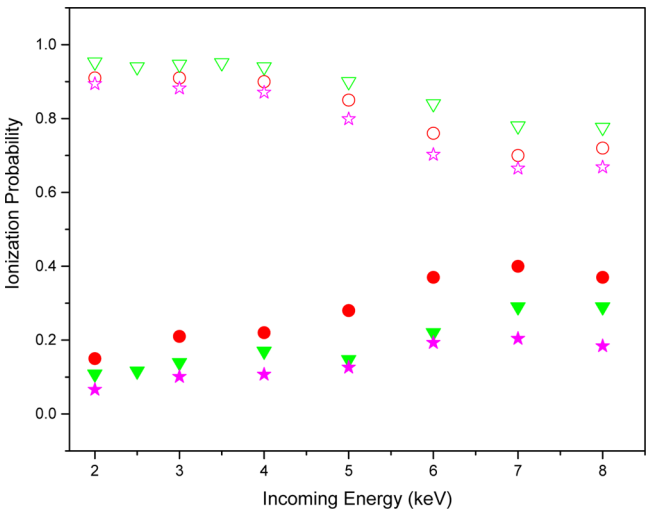

Figure 8. Ionization probabilities as a function of the incoming energy. Stars: trajectory (45°/90°) with all the interacting C atoms in expansion 4.1 and only diagonal on-site terms of eq 4.2. Green triangles: trajectory (90°/90°) with four C atoms in expansion 4.1 and only diagonal on-site terms of eq 4.2. Circles: trajectory (90°/90°) with four C atoms in expansion 4.1 and including also the off-diagonal on-site terms of eq 4.2. Full/empty symbols correspond to negative/positive ionization probabilities.

(90°/90°) trajectory with the correct perpendicular component of the incoming energy and only four C atoms in the expansion 4.1 compares well with the calculation that considers a real trajectory (45°/90°) and all the C atoms that the proton can *see* (interact with) in the expansion 4.1. These ionization probabilities, by using eq 3.2, lead to the ion fractions shown in Figure 4. Only the diagonal on-site terms of the density matrix (eq 4.2) have been taken into account in both calculations. In the same figure we can appreciate the influence of the density matrix off-diagonal on-site terms when considering only four C atoms interacting with the proton. As expected, the charge exchange is more sensitive to the interference effects due to the crossed terms of the density matrix, in the case of atom levels closer to the Fermi level.

The details of the small- and large-U limit approximations are given in the Supporting Information.

5. CONCLUSIONS

In summary, the analysis performed in each experimental setup shows that in spite of the similar ion fractions obtained in both FS and BS the physics is quite different. In the FS the slow perpendicular motion along the incoming path leads to an effective neutralization of the proton and then to a positive or negative ionization along the exit trajectory, where the infinite correlation limit provides an appropriate scenario. In the BS the level width introduced by the proton rapid motion begins to play an important role by diminishing the effective Coulomb repulsion U^*. The small-U limit is the adequate approximation to describe the experiments in this case. However, when the velocity is large enough to introduce an energy uncertainty such that the ionization and affinity levels are not well resolved, the adiabatic level shifts are not valid anymore, and the assumption of constant energy levels ($\varepsilon_I;\varepsilon_I + U$) provides a precise description of the ion fractions experimentally observed.

The distinctive conditions where the present analysis is valid are a consequence of not only the experimental setup or the incoming energy range but also of the nature of the system (H-HOPG) studied. Hydrogen one-electron ionization and affinity levels are close enough to each other to be fairly sensitive to the energy uncertainty widths, and also, they are located relatively close to the HOPG Fermi level, within the broadening introduced by the time evolution. The role played by the surface is essentially connected with the presence and magnitude of the density of states (DOS) in the surroundings of the projectile affinity and ionization levels.

■ ASSOCIATED CONTENT

Supporting Information

Additional theoretical details on small-U limit approximation and large-U limit approximation. This material is available free of charge via the Internet at http://pubs.acs.org.

■ AUTHOR INFORMATION

Corresponding Author

*Tel.: +54-342-4559175. Fax: +54-342-4550944. E-mail: bonetto@santafe-conicet.gov.ar.

Notes

The authors declare no competing financial interest.

■ ACKNOWLEDGMENTS

This work was supported by ANPCyT through PICT grants, CONICET through PIP grants, and U.N.L. through CAI+D grants.

■ REFERENCES

(1) Boers, A. L. Charge State of Low Energy Reflected Alkalis. *Nucl. Instrum. Methods Phys. Res. Sect. B* **1984**, *2*, 353−359.

(2) Los, J.; Geerlings, J. J. C. Charge Exchange in Atom-Surface Collisions. *Phys. Rep.* **1990**, *190*, 133−143.

(3) Ashwin, M. J.; Woodruff, D. P. Charge Exchange Processes in Li+ and He+ Ion Scattering from Alkali Adsorbates on Cu(110). *Surf. Sci.* **1991**, *244*, 247−258.

(4) German, K. A. H.; Weare, C. B.; Varekamp, P. R.; Andersen, J. N.; Yarmoff, J. A. Site-Specific Neutralization of Low Energy $^7Li^+$ Scattered from Na/Al(100). *Phys. Rev. Lett.* **1993**, *70*, 3510−3513.

DOI: 10.1021/jp511339v
J. Phys. Chem. C XXXX, XXX, XXX−XXX

(5) Kimmel, G. A.; Cooper, B. H. Dynamics of Resonant Charge Transfer in Low-Energy Alkali-Metal-Ion Scattering. *Phys. Rev. B* **1993**, *48*, 12164.
(6) Marston, J. B.; Andersson, D. R.; Behringer, E. R.; Cooper, B. H.; DiRubio, C. A.; Kimmel, G. A.; Richardson, C. Many-Body Theory of Charge Transfer in Hyperthermal Atomic Scattering. *Phys. Rev. B* **1993**, *48*, 7809.
(7) Behringer, E. R.; Andersson, D. R.; Cooper, B. H.; Marston, J. B. Charge Transfer in Hyperthermal Energy Collisions of Li^+ with Alkali-Metal-Covered Cu(001). I. Dynamics of Charge State Formation. *Phys. Rev. B* **1996**, *54*, 14765−14779.
(8) Borisov, A. G.; Teillet-Billy, D.; Gauyacq, J. P.; Winter, H.; Dierkes, G. Resonant Charge Transfer in Grazing Scattering of Alkali-Metal Ions from an Al(111) Surface. *Phys. Rev. B* **1996**, *54*, 17166−17174.
(9) Weare, C. B.; Yarmoff, J. A. Resonant Neutralization of 7Li+ Scattered from Alkali/Al(100) as a Probe of the Local Electrostatic Potential. *Surf. Sci.* **1996**, *348*, 359−369.
(10) Borisov, A. G.; Kazansky, A. K.; Gauyacq, J. P. Finite Time Effect in the Charge Transfer Process During an Ion-Metal Surface Collision. *Phys. Rev. Lett.* **1998**, *80*, 1996−1999.
(11) Goryunov, D. G.; Borisov, A. G.; Makhmetov, G. E.; Teillet-Billy, D.; Gauyacq, J. P. Li+ Neutralisation in Back-Scattering from Alkali/Al(100) Surfaces: Comparison between the Various Alkalis. *Surf. Sci.* **1998**, *401*, 206−219.
(12) Borisov, A. G.; Kazansky, A. K.; Gauyacq, J. P. Resonant Charge Transfer in Ion−Metal Surface Collisions: Effect of a Projected Band Gap in the H^-−Cu(111) System. *Phys. Rev. B* **1999**, *59*, 10935−10949.
(13) Hecht, T.; Winter, H.; Borisov, A. G.; Gauyacq, J. P.; Kazansky, A. K. Role of 2d Surface State Continuum and Projected Band Gap in Charge Transfer in Front of a Cu(111) Surface. *Phys. Rev. Lett.* **2000**, *84*, 2517.
(14) Yarmoff, J. A.; Yang, Y.; Liu, G. F.; Chen, X.; Sroubek, Z. Charge Exchange in Low-Energy Ion-Surface Scattering. *Vacuum* **2004**, *73*, 25.
(15) Canário, A. R.; Borisov, A. G.; Gauyacq, J. P.; Esaulov, V. A. Nonadiabatic Effects in Atom-Surface Charge Transfer. *Phys. Rev. B* **2005**, *71*, 121401.
(16) Garcia, E. A.; Gonzalez Pascual, C.; Bolcatto, P. G.; Passeggi, M. C. G.; Goldberg, E. C. Ion Fractions in the Scattering of Hydrogen on Different Reconstructed Silicon Surfaces. *Surf. Sci.* **2006**, *600*, 2195.
(17) Wiatrowsky, M.; Lavagnino, N.; Esaulov, V. A. Li+ Ion Neutralization on Ag Layers Grown on Cu(1 1 1). *Surf. Sci. Lett.* **2007**, *601*, L39.
(18) Bonetto, F.; Romero, M. A.; Garcia, E. A.; Vidal, R. A.; Ferrón, J.; Goldberg, E. C. Large Neutral Fractions in Collisions of Li+ with a Highly Oriented Pyrolytic Graphite Surface: Resonant and Auger Mechanisms. *Phys. Rev. B* **2008**, *78*, 075422.
(19) Hamoudi, H.; Dablemont, C.; Esaulov, V. A. Interaction of Li+ with a Au(100) Surface. *Surf. Sci.* **2008**, *302*, 2486.
(20) Garcia, E. A.; Romero, M. A.; Gonzalez Pascual, C.; Goldberg, E. C. Neutralization of Li+ Ions Scattered by the Cu (100) and (111) Surfaces: A Localized Picture of the Atom-Surface Interaction. *Surf. Sci.* **2009**, *603*, 597−605.
(21) Chen, L.; Shen, J.; Jia, J.; Kandasamy, T.; Bobrov, K.; Guillemot, L.; Fuhr, J. D.; Martiarena, M. L.; Esaulov, V. A. Li+-Ion Neutralization on Metal Surfaces and Thin Films. *Phys. Rev. A* **2011**, *84*, 052901.
(22) Vidal, R. A.; Bonetto, F.; Ferrón, J.; Romero, M. A.; Garcia, E. A.; Goldberg, E. C. Electron Captureand Loss in the Scatteringof H+ from Hopg Graphite. *Surf. Sci.* **2011**, *605*, 18.
(23) Meyer, C.; Bonetto, F.; Vidal, R.; García, E. A.; Gonzalez, C.; Ferrón, J.; Goldberg, E. C. Understanding the High Neutralization Yields in Collisions of K_{ev} Li^+ Ions with Copper Surfaces. *Phys. Rev. A* **2012**, *86*, 032901.
(24) Romero, M. A.; Iglesias-García, A.; Goldberg, E. C. Quantum-Mechanical Interference in Charge Exchange between Hydrogen and Graphene-Like Surfaces. *J. Phys.: Condens. Matter* **2012**, *24*, 045004.
(25) Bonetto, F.; Romero, M. A.; Garcia, E. A.; Vidal, R. A.; Ferrón, J.; Goldberg, E. C. Relevant Effects of Localized Atomic Interactions and Surface Density of States on Charge Transfer in Ion-Surface Collisions. *Europhys. Lett.* **2007**, *80*, 53002.
(26) Bonetto, F. J.; García, E. A.; González, C.; Goldberg, E. C. Image Potential State Influence on Charge Exchange in Li+−Metal Surface Collisions. *J. Phys. Chem. C* **2014**, *118*, 8359−8368.
(27) Iglesias-García, A.; Bonetto, F.; Vidal, R.; Ferrón, J.; Goldberg, E. C. Ion Neutralization and High-Energy Electron Emission in He+ Scattering by a Highly Oriented Pyrolitic Graphite Surface. *Phys. Rev. A* **2014**, *89*, 042702.
(28) Tsumori, K.; Koppers, W. R.; Heeren, R. M. A.; Kadodwala, M. F.; Beijersbergen, J. H. M.; Kleyn, A. W. Large Ion Yields in Hydrogen Scattering from a Graphite Surface. *J. Appl. Phys.* **1997**, *81*, 6390−6396.
(29) Wada, M.; Kenmotsu, T.; Matsumoto, Y.; Nishiura, M.; Sasao, M.; Tsumori, K.; Yamaoka, H. Low-Energy Particle Interaction with Plasma-Irradiated Metal Surfaces. *Plasma Devices Oper.* **2009**, *17*, 132−143.
(30) Tanaka, N.; Kato, S.; Miyamoto, T.; Nishiura, M.; Tsumori, K.; Matsumoto, Y.; Kenmotsu, T.; Okamoto, A.; Kitajima, S.; Sasao, M.; Wada, M.; Yamaoka, H. Effects of Roughness and Temperature on Low-Energy Hydrogen Positive and Negative Ion Reflection from Silicon and Carbon Surfacesa). *Rev. Sci. Instrum.* **2014**, *85*, -.
(31) Gleeson, M. A.; Kleyn, A. W. Effects of Cs-Adsorption on the Scattering of Low Energy Hydrogen Ions from Hopg. *Nucl. Instrum. Methods Phys. Res. Sect. B* **1999**, *157*, 48−54.
(32) Souda, R.; Asari, E.; Kawanowa, H.; Suzuki, T.; Otani, S. Capture and Loss of Valence Electrons During Low Energy H+ and H− Scattering from Lab6(100), Cs/Si(100), Graphite and Licl. *Surf. Sci.* **1999**, *421*, 89−99.
(33) Luna, N. B.; Bonetto, F. J.; Vidal, R. A.; Goldberg, E. C.; Ferrón, J. Low Energy Ion Scattering in He/Hopg System. *J. Mol. Catal. A: Chem.* **2008**, *281*, 237−240.
(34) Chen, L.; Ding, B.; Li, Y.; Qiu, S.; Xiong, F.; Zhou, H.; Guo, Y.; Chen, X. Evidence for the Incoming-Velocity Effect on Negative Fluorine Ions Scattering from a Highly-Oriented-Pyrolytic-Graphite Surface. *Phys. Rev. A* **2013**, *88*, 044901.
(35) Datta, D.; Shen, J.; Esaulov, V. A. Hydrogen Negative Ion Formation on a Graphite Hopg Surface. *Nucl. Instrum. Methods Phys. Res. Sect. B* **2013**, *315*, 42−44.
(36) Nordlander, P.; Tully, J. C. Energy Shifts and Broadening of Atomic Levels near Metal Surfaces. *Phys. Rev. B* **1990**, *42*, 5564.
(37) Brongersma, H. H.; Draxler, M.; de Ridder, M.; Bauer, P. Surface Composition Analysis by Low-Energy Ion Scattering. *Surf. Sci. Rep.* **2007**, *62*, 63.
(38) Bhattacharya, R. S.; Eckstein, W.; Verbeek, H. Positive Charge Fractions of H, D, and He Backscattered from Solid Surfaces. *Surf. Sci.* **1980**, *93*, 563−581.
(39) Verbeek, H.; Eckstein, W.; Bhattacharya, R. S. Negative Hydrogen Ion Formation by Backscattering from Solid Surfaces. *Surf. Sci.* **1980**, *95*, 380−390.
(40) Bonetto, F.; García, E. A.; Vidal, R.; Ferrón, J.; Goldberg, E. C. Experimental and Theoretical Study of Charge Transfer in Hydrogen Ion Scattering from a Graphite Surface. *Appl. Surf. Sci.* **2007**, *254*, 62−64.
(41) Anderson, P. W. Localized Magnetic States in Metals. *Phys. Rev.* **1961**, *124*, 41−53.
(42) Keldysh, L. V. Diagram Technique for Nonequilibrium Processes. *Sov. Phys. JETP* **1965**, *20*, 1018.
(43) Grizzi, O.; Shi, M.; Bu, H.; Rabalais, J. W. Time-of-Flight Scattering and Recoiling Spectrometer (Tof-Sars) for Surface Analysis. *Rev. Sci. Instrum.* **1990**, *61*, 740.
(44) Cohen-Tannoudji, C.; Diu, B.; Laloe, F. *Quantum Mechanics*; Wiley: New York, 1991; Vol. *1*.
(45) Mott, N. F.; Massey, H. S. W. *The Theory of Atomic Collisions*; Oxford University Press: New York, 1965.
(46) Romero, M. A.; Flores, F.; Goldberg, E. C. Effective Treatment of Charge and Spin Fluctuations in Dynamical and Static Atom-Surface Interactions. *Phys. Rev. B* **2009**, *80*, 235427.

DOI: 10.1021/jp511339v
J. Phys. Chem. C XXXX, XXX, XXX−XXX

(47) Goldberg, E. C.; Flores, F. Charge Exchange in Many-Body Time-Dependent Processes. *Phys. Rev. B* **1992**, *45*, 8657−8664.
(48) Goldberg, E. C.; Passeggi, M. C. G. Correlation Effects in Dynamical Charge-Transfer Processes. *J. Phys.: Condens. Matter* **1993**, *5*, A259.
(49) Bolcatto, P. G.; Goldberg, E. C.; Passeggi, M. C. G. Interaction between Atoms and Surfaces: A Bond-Pair Description Based on an Extended Anderson Model. *Phys. Rev. B* **1998**, *58*, 5007.

DOI: 10.1021/jp511339v
J. Phys. Chem. C XXXX, XXX, XXX−XXX